Longitudinal and Transverse Instability of Ion Acoustic Waves

T. Chapman, R. L. Berger, B. I. Cohen, J. W. Banks, and S. Brunner

Longitudinal and transverse instability of ion acoustic waves

T. Chapman,* R. L. Berger, and B. I. Cohen

Lawrence Livermore National Laboratory, P.O. Box 808, Livermore, CA 94551, USA

J. W. Banks

Department of Mathematical Sciences, Rensselaer Polytechnic Institute, 301 Amos Eaton Hall, Troy, NY 12180, USA

S. Brunner

Swiss Plasma Centre, École Polytechnique Fédérale de Lausanne, Station 13, CH-1015 Lausanne, Switzerland

Ion acoustic waves are found to be susceptible to at least two distinct decay processes. Which process dominates depends on parameters. In the cases examined, the decay channel where daughter modes propagate parallel to the mother mode is found to dominate at larger amplitudes, while the decay channel where the daughter modes propagate at angles to the mother mode dominates at smaller amplitudes. Both decay processes may occur simultaneously and with onset thresholds below those suggested by fluid theory, resulting in the eventual multi-dimensional collapse of the mother mode to a turbulent state.

Ion acoustic waves (IAWs) in plasma are susceptible to decay processes. With weak or absent damping[1], an IAW can decay to daughter IAWs. Using simulation techniques novel in the study of IAWs, we find IAWs are unstable via at least two distinct decay mechanisms, with a threshold for instability far below fluid theory and a decay mode growth rate significantly faster than fluid theory. Which decay process dominates in the linear phase of instability is dependent on parameters. We find that other properties of IAW decay, such as the direction of propagation of the dominant decay modes, do not conform to existing theory.

IAWs may be excited by a variety of mechanisms under controlled laboratory experiments and during inertial confinement fusion (ICF) experiments. In typical ICF designs, laser light must propagate through high-gain plasma and overlap with multiple crossing laser beams. Understanding the onset and saturation of stimulated Brillouin scattering (SBS) and crossed-beam energy transfer[2, 3] mediated by IAWs is vital to designing successful experiments and avoiding optics damage[4, 5]. Ongoing efforts to model laser-plasma interaction in ICF experiments[6] with linear plasma wave descriptions require clamps on IAW amplitudes, suggesting IAW nonlinearity. Experimentally, IAW decay has been correlated with SBS saturation[7] and off-axis decay modes have been observed[8].

In the following, we demonstrate for the first time the decay of IAWs to daughter modes via multiple distinct channels using a fully-kinetic numerical treatment. Such a treatment is necessary to describe correctly the impact of particle trapping on the evolution of the IAWs, including nonlinear wave couplings, dampings, and frequencies. Our collisionless and noiseless (to machine precision) Vlasov simulations are 2D+2V (two configuration space + two velocity space dimensions). The results obtained reveal a picture of IAW decay that is qualitatively different from previous 2D numerical[9–13] and theoretical[12–14] treatments where the electrons were not treated as kinetic, reveal decay processes not captured by fully kinetic 1D simulations[15–18], and allow measurement of linear growth rates not possible in previous fully kinetic 2D/3D simulations[19] due to discrete particle noise.

Our results show two clearly distinct IAW decay channels, with daughter waves characterized by differing wave numbers $\mathbf{k} = (k_\parallel, k_\perp)$, where subscripts indicated orientation relative to the mother wave: i) Daughter waves with $k_\perp = 0$ and a growth rate that peaks at $k_\parallel = k_1/2$, where $\mathbf{k_{(1,0)}} = (k_1, 0)$ is the wave number of the mother wave. This resonant three-wave process is known as two-ion wave decay (TID)[20]. ii) Daughter waves with a growth rate that peaks at $|k_\perp| > 0$ and $k_\parallel = k_1$, which we refer to here as off-axis instability (OAI). In the following, modes are distinguished by a subscript l (not necessary an integer) that indicates a quantity relative to the mother mode, e.g., $k_l = lk_1$ and $\mathbf{k_{(l,m)}} = (k_l, k_m)$.

This Letter is organized as follows: First, we briefly describe our numerical method. Next, we use a single case to illustrate the various processes taking place during IAW decay. Afterwards, the scaling of the decay processes are discussed.

In order to study IAW decay, we use the Vlasov code LOKI[21–23], which employs 4th-order-accurate, conservative, finite difference algorithms in 2D+2V space, with variables time t, space $\mathbf{r} = (x, y)$, and velocity $\mathbf{v} = (v_x, v_y)$. The plasma is periodic in both spatial dimensions (directions $\hat{\mathbf{x}}$ and $\hat{\mathbf{y}}$). Both electrons (e) and ions (i) are described using continuum representations of their respective distribution functions $f_j = f_j(t, \mathbf{r}, \mathbf{v})$ where $j = e, i$. f_j is initialized as a spatially homogeneous 2D Maxwellian, $f_{j0} = f_{j0}(\mathbf{v}) = [1/(2\pi v_{tj}^2)] \exp[-\mathbf{v}^2/2]$, with initial temperature T_j and thermal velocity $v_{tj} = \sqrt{T_j/m_j}$, where m_j is the mass of species j. The meshes are uniform, with spacings for each species no coarser than $\Delta x = 0.44\lambda_{De}$, $\Delta y = 3.1\lambda_{De}$, $\Delta v_x = 0.21v_{tj}$,

$\Delta v_y = 0.25 v_{tj}$, while the time step Δt of the explicit scheme satisfies a Courant-Friedrichs-Lewy condition (typically, $\Delta t \sim 0.04/\omega_{pe}$, where ω_{pe} is the electron plasma frequency). The velocity domain of f_j is truncated such that $v_{x,y} \in [-8v_{tj}, 8v_{tj}]$, or, in the case of the positive v_x boundary for the ions, whatever is necessary to comfortably contain the phase velocity plus the ion trapping half-width (up to $\sim 20v_{ti}$). A characteristic velocity boundary condition is applied[22]. The computational burden of the simulations presented here is significant: owing to the 4D phase space and the need to resolve electron kinetic physics over a timescale dictated by the ions, our largest simulations shown here required $\sim 1 \times 10^9$ mesh points and $\sim 2 \times 10^6$ time steps (equivalent to a duration $\sim 10^5/\omega_{pe}$). Convergence of our numerical results was checked by various numerical resolution studies and further by increasing the order of the numerical scheme from 4 to 6.

We present first a single illustrative example of an IAW through excitation, BGK-like[24] propagation, and then decay into a turbulent spectrum of daughter modes through multiple channels. The minimum set of dimensionless parameters needed to describe linear IAWs is ZT_e/T_i, Zm_e/m_i, and $k\lambda_{De}$, where λ_{De} is the electron Debye length. For numerical efficiency, the plasma is chosen here to be fully ionized hydrogen (charge $Z = 1$). We use a physical mass ratio such that $Zm_i/m_e = 1836$, and here select $ZT_e/T_i = 8$ and $k_1\lambda_{De} = 0.4$ (effective parameters typical of those in, e.g., ICF experiments). A plane wave with frequency $\omega \approx \omega_1^L = 0.469\omega_{pi}$ and wave number $\mathbf{k} = (k_1, 0)$ is excited parallel to $\hat{\mathbf{x}}$ in a system with length $L_x = 8\lambda_1 \approx 126\lambda_{De}$ by a spatially and temporally sinusoidal driver resonant with the linear mother IAW, where the wave length λ is given by $\lambda = 2\pi/k$. ω_{pi} is the ion plasma frequency and the superscript L denotes a linear mode frequency; NL (used later) denotes the actual (amplitude-dependent) nonlinear mode frequency. The system is chosen to be of width $L_y = 38.4\lambda_1 \approx 600\lambda_{De}$.

The electrostatic energy U_{ES} of the system increases while the wave is driven, as shown in Fig. 1(a); the driver field E_D is applied to the electrons and ramped up to $e\lambda_{De}E_D/T_e = 0.0175$ and down to zero across the gray region. After the driver is switched off at $\omega_{pi}t \approx 200$, U_{ES} is nearly constant apart from fast-timescale oscillations due to trapped ions exchanging energy with the wave. The wave continues in a BGK-like state until $\omega_{pi}t \sim 1.35 \times 10^3$, at which point U_{ES} crashes and does not recover. Snapshots of the electric potential energy Φ are shown in Figs. 1(b-e). After the driver is switched off but before the crash in U_{ES}, the envelope amplitude of Φ is $|e\phi/T_e| \sim 0.15$.

In Fig. 1(b), the wave is still in an approximately plane λ_1-periodic state, although multiple nonlinear effects are present. Particle trapping (both electrons and ions) results in a modified (qualitatively flattened) distribution function in the region of velocity space resonant with

$v_1 = \omega_1/k_1$ (this resonance half-width is given analytically by $v_{tr,j}/v_{tj} = 2\sqrt{Z_j e\phi/T_j}$). This modification results in a nonlinear frequency shift away from ω_1^L that is negative in this case[25–27] (quantified later), reduced or
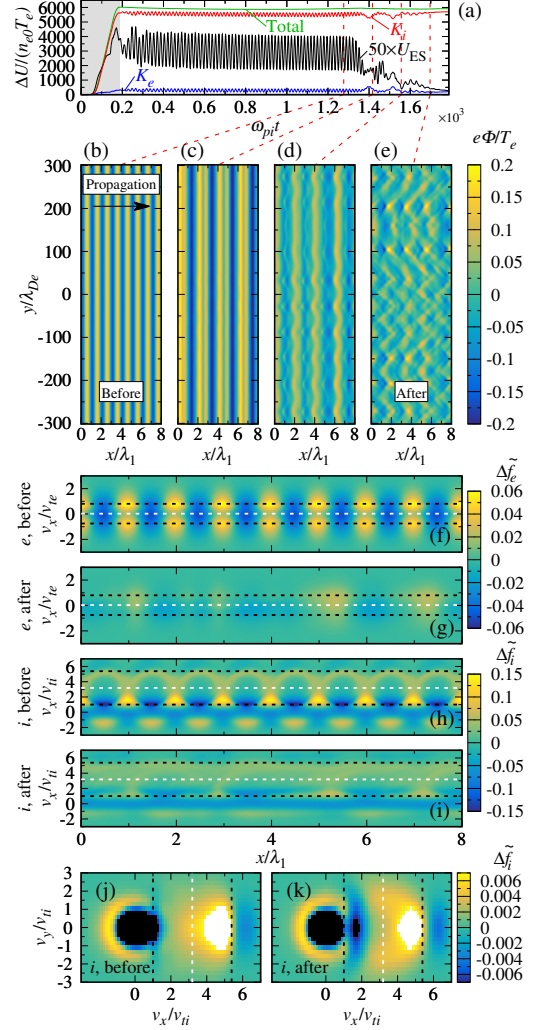

FIG. 1. $ZT_e/T_i = 8$, $k\lambda_{De} = 0.4$, $Zm_e/m_i = 1/1836$ (H plasma). (a) Evolution of the electrostatic (U_{ES}), electron kinetic (K_e) and ion kinetic (K_i) energies. The driven (undriven) period is colored gray (white). (b-e) Snapshots of the IAW potential Φ before, during, and after the crash in electrostatic energy. The half-harmonic ($\lambda = 2\lambda_1$) is the dominant mode during the crash. The distribution functions $f_{e,i}$ in (f-k) are snapshots shown as deviations from Maxwellian $f_{e,i}^M$, taken before (f,h,j) and after (g,i,k) the crash in U_{ES} at times indicated by the leftmost and rightmost red dashed lines in (a), respectively. Shown are: (f,g) $\Delta\tilde{f}_e = (v_{te}/n_{e0})\int(\langle f_e\rangle_y - f_{e0})\,dv_y$; (h,i) $\Delta\tilde{f}_i = (v_{ti}/n_{i0})\int(\langle f_i\rangle_y - f_{i0})\,dv_y$; and (j,k) $\Delta\tilde{f}_i = (v_{ti}^2/n_{i0})(\langle f_i\rangle_{x,y} - f_{i0})$. $\langle\ldots\rangle_a$ indicates an averaging over the dimension(s) a. White dashed lines in (f-k) indicate the measured nonlinear phase velocity $v_1 = \omega_1/k_1$ of the fundamental mode, while black dashed lines show analytic estimates of the species trapping widths, $v_1 \pm v_{tr,j}$.

completely eliminated Landau damping[1], and harmonic generation (wave steepening) producing $l = 2, 3, \ldots$ modes larger than predicted by fluid theory[17, 27], which also contribute to the nonlinear frequency.

In Fig. 1(c), the decay modes have grown to the point that the periodicity of the wave has changed from λ_1 to $\sim\lambda_{1/2}$: the so-called half-harmonic [$l = 1/2$, $\mathbf{k} = (k_1/2, 0)$] of the $l = 1$ mode is briefly dominant, having grown faster than all other decay modes (discussed quantitatively later). Despite there still being a dominant IAW mode, U_{ES} has already begun to decrease at this point, which we attribute to wave-particle effects, such as the loss of previously trapped particles from the wave and the work done by the wave as the distribution functions respond to the changing wave potential. Accounting for the k-dependent sloshing energy of the electrons and ions as the spectrum evolves does not explain the loss of U_{ES} (see, e.g., Refs. 14, 16, or 18).

In Figs. 1(d) and 1(e), the IAW mode spectrum becomes increasingly turbulent, and modes with $|k_\perp| > 0$ are significant. The resulting transverse modulation of the potential gives rise to wave front bowing, the negative nonlinear frequency shift causing a retardation of higher-amplitude phase fronts, and perhaps self-focusing[19, 22, 28]. U_{ES} tends to zero, similar to the behavior seen in 1D systems[17], with dwindling soliton-like localized wave packets.

The oscillations in electrostatic energy U_{ES} reflect an exchange primarily with trapped particles; the resultant oscillation in electron and ion kinetic energies, K_e and K_i, is shown in Fig. 1(a), as well as the total energy (quiescent kinetic energies have been subtracted). After the onset of turbulence, electrostatic energy is lost primarily to the ions. The distribution functions are altered significantly by the transition to a turbulent state. The loss of periodicity in f_e and f_i is readily apparent in Figs. 1(f-i), where snapshots of f_j are taken pre- and post-turbulence at the times indicated in Figs. 1(a) (leftmost and rightmost red vertical dashed lines, respectively). Particles are released from λ_1-periodic orbits along v_x [the separatrix between passing and trapped trajectories is evident in Figs. 1(f) and 1(h)] and the distribution becomes washed-out after the onset of turbulence. The growth of OAI modes also acts to smear f_j along v_y: f_i averaged over space is shown in Figs. 1(j) and 1(k) at the same pre- and post-turbulent times, exhibiting a clear transverse acceleration of trapped ions.

The evolution of the Fourier modes corresponding to the mother and fastest-growing daughter modes driven by TID and OAI are shown in Fig. 2(a) for the case shown in Fig. 1. The linear decay mode growth rates $\gamma(k_x, k_y)$ [measured by taking exponential fits, as in the black dashed line in Fig. 2(a)] are shown in Fig. 2(b) and accompanying real frequencies in Fig. 2(c). We observe two distinct instabilities of the initially near-monochromatic ($l = 1$ mode) IAW: a purely longitudinal

instability known as TID[20] for which $\gamma = \gamma(k_x, 0)$, and transverse modulational-type instability referred to here as OAI where $\gamma = \gamma(k_x, |k_y| > 0)$. A spatially 1D system that permits spatial variation along only the direction of propagation of the mother wave recovers the same linear TID growth rate as the 2D system shown here in Fig. 2(d), but does not permit OAI (this was confirmed by comparing 1D and 2D simulations). As in related 1D studies[17, 29], Bloch-Floquet type eigenmodes are present [i.e., $\gamma(k_x, 0)$ is symmetric about k_n over the interval ($[n - 1/2]k_1, [n + 1/2]k_1$), where $n = 1, 2, \ldots$, with period k_1], conforming to the linear stability analysis of periodic waves by Goldman[30].

The hallmark of TID is a decay mode growth rate that peaks at the half-harmonic. This decay channel is dominant in this example of IAW decay, and is responsible for the transition from a system dominated by the $l = 1$ mode shown in Fig. 1(b) to a system dominated by the $l = 1/2$ mode shown in Fig. 1(c). The growth rate in simulations exceeds estimates from fluid theory[20] by a factor of ~3 in this case[17].

While slower in this case than TID, the OAI growth rate is still significant and peaks at $k_x\lambda_{De} = k_1\lambda_{De} = 0.4$ and $k_y\lambda_{De} \sim 0.1$, although varying weakly with k_x. Similarly to TID, the OAI occurring for modes with growth rates $\gamma(k_1, k_y)$ measured here and shown in Fig. 2(e) may
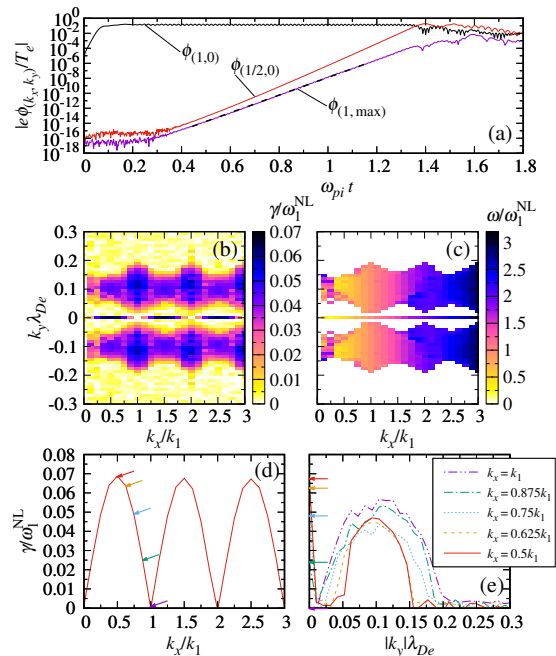

FIG. 2. Fourier space analysis of the case presented in Fig. 1. (a) Fourier mode evolution of the mother and fastest-growing daughter modes corresponding to TID and OAI. (b) Linear (pre-turbulence) growth rates $\gamma = \gamma(k_x, k_y)$. (c) Mode frequencies $\omega = \omega(k_x, k_y)$. (d) TID growth rate, $\gamma = \gamma(k_x, 0)$. (e) Slices showing γ for various fixed k_x. Arrows indicate identical modes in (d) and (e).

be recovered in a simpler system that is large in the transverse direction and only a single wavelength long ($L_x = \lambda_1$). Such a system does not support TID. However, in the systems considered here that are both large in the transverse direction and many wave lengths long, we observe the growth of modes with $\mathbf{k} = (k_x \neq k_1, |k_y| > 0)$ that can not be observed in simplified systems.

All decay modes in the linear phase of growth have frequencies $\omega \approx (k_x/k_1)\omega_1$, as seen in Fig. 2(c). Decay mode frequencies appear to be independent of k_y. The mode frequency was calculated by taking the time derivative of the phase of the complex mode amplitude after a 2D Fourier transform in space, here averaged over the interval $\omega_{pi}t = [1 \times 10^3, 1.3 \times 10^3]$; this method is more approximate than the Hilbert transform method[27] used to extract ω_1^{NL}, the nonlinear mother mode frequency, but adequate to determine the overall behavior of $\omega(k_x, k_y)$.

The scaling of γ with $|\phi_1|$, the potential of the mode $\mathbf{k} = (k_1, 0)$, is shown in Fig. 3(a), generated by exciting mother IAWs of various amplitudes and measuring γ in each case. For these parameters ($ZT_e/T_i = 8$, $Zm_e/m_i = 1/1836$, $k_1\lambda_{De} = 0.4$), TID (vertical cross points) is the dominant decay mechanism for $|e\phi_1/T_e| \gtrsim 0.025$, as is the case in Fig. 1 where $|e\phi_1/T_e| \approx 0.15$. For OAI, γ is consistently greatest at $k_x = k_1$ (diamond points), and scales similarly with $|\phi_1|$ for all k_x. At $|e\phi_1/T_e| \approx 0.025$, γ is similar across all decay channels. For $|e\phi_1/T_e| \lesssim 0.025$, TID is slower than OAI and at $|e\phi_1/T_e| = 0.011$ TID is below threshold and does not occur.

The TID daughter modes share identical phase velocities to the mother mode due to the one-dimensional nature of the three-wave decay, matching conditions for frequency and wave number, and the acoustic dispersion of IAWs. The trapping-induced flattening of the distribution function caused by the mother mode therefore suppresses Landau damping of the daughter modes also. Neglecting trapping, a threshold for TID based on

FIG. 3. Analysis of cases with the same parameters as Fig. 1 but varying mother wave amplitudes (horizontal axis). (a) Scaling of γ with $|\phi_1|$ for TID and OAI. The gray horizontal line indicates the linear Landau damping rate of the $l = 1/2$ mode, $\nu_{1/2}$. (b) The scaling of k_y for the fastest growing mode for OAI with $|\phi_1|$ (left vertical axis) and the scaling of the nonlinear frequency shift $\Delta\omega_1^{NL} = \omega_1^{NL} - \omega_1^L$ with $|\phi_1|$ (right vertical axis).

a linear Landau damping rate of the $l = 1/2$ mode[20] $\nu_{1/2} = 0.043\omega_{1/2}^L$ suggests a TID amplitude threshold ϕ_1^{tr} of $|e\phi_1^{tr}/T_e| \approx 0.09$. A threshold arising from the nonlinear scaling of ω with k from the fluid theory of IAWs suggests[17] $|e\phi_1^{tr}/T_e| \approx 0.04$. Such descriptions of TID are clearly insufficient, as observed previously[17]. We have not observed a threshold for OAI at $k_x = k_1$.

In Fig. 3(b), the scaling of k_y with $|\phi_1|$ for the fastest-growing OAI mode, $\mathbf{k} = \mathbf{k}_{(1,\max)} = (k_1, k_y^{\max})$, is shown (left vertical axis). The sidebands of OAI move further in $|k_y|$ from the mother IAW as $|\phi_1|$ is increased. The scaling of the nonlinear frequency shift $\Delta\omega_1^{NL} = \omega_1^{NL} - \omega_1^L$ with $|\phi_1|$ is also shown in Fig. 3(b) (right vertical axis). In this case, the opposing electron and ion contributions to the trapping-induced nonlinear frequency shift expected from nonlinear analysis[27] almost cancel, and indeed the overall shift is small until $|e\phi_1/T_e| \gtrsim 0.1$.

Previous attempts[12–14] at deriving a multi-dimensional theory of IAW decay have not included explicit electron kinetic effects, although Ref. [14] permitted an arbitrary frequency shift that could be taken to include an electron contribution. None of these substantial works appears to capture the decay properties observed here, such as the consistent presence of TID and OAI, and the relatively weak dependence of the growth rate of OAI modes on k_x/k_1. One can write down a Schrödinger-type equation for IAWs describing transverse instability similar to that studied in Ref. 31 for longitudinal instability (see, e.g., Ref. 32). Such a model is based on the total frequency shift of the mother mode, $\Delta\omega_1^{NL}$. With IAWs, it is possible to measure $\Delta\omega_1^{NL} \simeq 0$ for finite $|\phi_1|$ due to the opposite signs of the contributions from electrons and ions. Indeed, this is the case in Fig 3 for $|e\phi_1/T_e| \lesssim 0.025$, and yet a transverse instability is observed.

Perhaps a more likely candidate for an off-axis instability mechanism is an ion-driven trapped particle instability (TPI) akin to that observed in the longitudinal direction unambiguously in electron plasma waves (EPWs) in 1D[29, 33] (we emphasize ion-driven, since the electron bounce frequency is very large compared to the IAW frequency, preventing resonance), which may also drive a transverse filamentation-like TPI in EPWs[32]. Our attempts to derive a TPI growth rate for IAWs analytically have not yielded results that agree with simulations. However, this and similar models of trapped particle instabilities typically assume i) that the initial state of the IAW can be considered mono-chromatic, while in actuality $|\phi_2|/|\phi_1| \sim 0.35$ for $|e\phi/T_e| = 0.15$, ii) that the trapped particles reside at the bottom of the potential well of the wave and have a single frequency, which for IAWs tends to be a rather poor approximation[27], and iii) that all trapping effects can be described perturbatively, which for the range of wave amplitudes studied here, may not be the case.

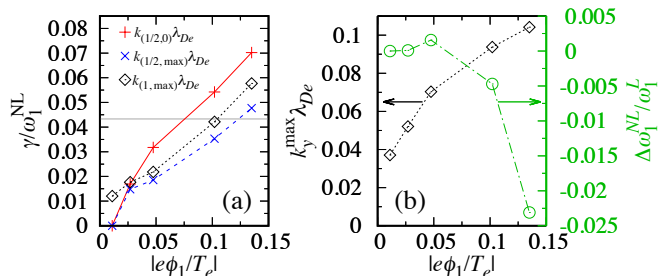In conclusion, we find ion acoustic waves exhibit at

least two distinct and competing decay processes. While a single decay process might lead to the initial break-up of the wave either transversely or longitudinally, once a nonlinear state is reached, breakup in both directions is typical. Which decay process dominates initially is dependent on parameters. Thresholds for instability do not agree with estimates based on linear (quiescent plasma) damping rates, and instability growth rates do not conform to existing theories.

———————

* email: chapman29@llnl.gov

[1] T. O'Neil, Phys. Fluids **8**, 2255 (1965).

[2] W. L. Kruer, S. C. Wilks, B. B. Afeyan, and R. K. Kirkwood, Phys. Plasmas **3**, 382 (1996), http://dx.doi.org/10.1063/1.871863.

[3] V. V. Eliseev, W. Rozmus, V. T. Tikhonchuk, and C. E. Capjack, Physics of Plasmas **3**, 2215 (1996), http://dx.doi.org/10.1063/1.871703.

[4] P. Michel, S. H. Glenzer, L. Divol, D. K. Bradley, D. Callahan, S. Dixit, S. Glenn, D. Hinkel, R. K. Kirkwood, J. L. Kline, W. L. Kruer, G. A. Kyrala, S. L. Pape, N. B. Meezan, R. Town, K. Widmann, E. A. Williams, B. J. MacGowan, J. Lindl, and L. J. Suter, Physics of Plasmas **17**, 056305 (2010), http://dx.doi.org/10.1063/1.3325733.

[5] J. D. Moody, P. Michel, L. Divol, R. L. Berger, E. Bond, D. K. Bradley, D. A. Callahan, E. L. Dewald, S. Dixit, M. J. Edwards, S. Glenn, A. Hamza, C. Haynam, D. E. Hinkel, N. Izumi, O. Jones, J. D. Kilkenny, R. K. Kirkwood, J. L. Kline, W. L. Kruer, G. A. Kyrala, O. L. Landen, S. LePape, J. D. Lindl, B. J. MacGowan, N. B. Meezan, A. Nikroo, M. D. Rosen, M. B. Schneider, D. J. Strozzi, L. J. Suter, C. A. Thomas, R. P. J. Town, K. Widmann, E. A. Williams, L. J. Atherton, S. H. Glenzer, and E. I. Moses, Nat Phys **8**, 344 (2012).

[6] D. J. Strozzi, D. S. Bailey, P. Michel, L. Divol, S. M. Sepke, G. D. Kerbel, C. A. Thomas, J. E. Ralph, J. D. Moody, and M. B. Schneider, Phys. Rev. Lett. **118**, 025002 (2017).

[7] H. C. Bandulet, C. Labaune, K. Lewis, and S. Depierreux, Phys. Rev. Lett. **93**, 035002 (2004).

[8] C. Niemann, S. H. Glenzer, J. Knight, L. Divol, E. A. Williams, G. Gregori, B. I. Cohen, C. Constantin, D. H. Froula, D. S. Montgomery, and R. P. Johnson, Phys. Rev. Lett. **93**, 045004 (2004).

[9] B. I. Cohen, B. F. Lasinski, A. B. Langdon, and E. A. Williams, Phys. Plasmas **4**, 956 (1997).

[10] C. Riconda, S. Hüller, J. Myatt, and D. Pesme, Phys. Scr., T **T84**, 217 (2000).

[11] L. Divol, B. I. Cohen, E. A. Williams, A. B. Langdon, and B. F. Lasinski, Phys. Plasmas **10**, 3728 (2003).

[12] B. I. Cohen, L. Divol, A. B. Langdon, and E. A. Williams, Phys. Plasmas **12**, 052703 (2005).

[13] B. I. Cohen, E. A. Williams, R. L. Berger, D. Pesme, and C. Riconda, Phys. Plasmas **16**, 032701 (2009), erratum: Phys. Plasmas **16**, 089902 (2009).

[14] D. Pesme, C. Riconda, and V. T. Tikhonchuk, Phys. Plasmas **12**, 092101 (2005), erratum: Phys. Plasmas **16**, 089903 (2009).

[15] C. Riconda, A. Heron, D. Pesme, S. Hüller, V. T. Tikhonchuk, and F. Detering, Phys. Rev. Lett. **94**, 055003 (2005).

[16] C. Riconda, A. Heron, D. Pesme, S. Huller, V. T. Tikhonchuk, and F. Detering, Phys. Plasmas **12**, 112308 (2005).

[17] T. Chapman, S. Brunner, J. W. Banks, R. L. Berger, B. I. Cohen, and E. A. Williams, Phys. Plasmas **21**, 042107 (2014).

[18] T. Chapman, B. J. Winjum, S. Brunner, R. L. Berger, and J. W. Banks, Phys. Plasmas **22**, 092116 (2015), http://dx.doi.org/10.1063/1.4930131.

[19] B. J. Albright, L. Yin, K. J. Bowers, and B. Bergen, Phys. Plasmas **23**, 032703 (2016), http://dx.doi.org/10.1063/1.4943102.

[20] S. J. Karttunen, J. N. McMullin, and A. A. Offenberger, Phys. Fluids **24**, 447 (1981).

[21] J. Banks and J. Hittinger, IEEE Trans. Plasma Sci. **38**, 2198 (2010).

[22] J. W. Banks, R. L. Berger, S. Brunner, B. I. Cohen, and J. A. F. Hittinger, Phys. Plasmas **18**, 052102 (2011).

[23] J. W. Banks, S. Brunner, R. L. Berger, and T. M. Tran, Phys. Plasmas **23**, 032108 (2016), http://dx.doi.org/10.1063/1.4943194.

[24] I. B. Bernstein, J. M. Greene, and M. D. Kruskal, Phys. Rev. **108**, 546 (1957).

[25] R. L. Dewar, Phys. Fluids **15**, 712 (1972).

[26] G. J. Morales and T. M. O'Neil, Phys. Rev. Lett. **28**, 417 (1972).

[27] R. L. Berger, S. Brunner, T. Chapman, L. Divol, C. H. Still, and E. J. Valeo, Phys. Plasmas **20**, 032107 (2013).

[28] J. W. Banks, R. L. Berger, T. Chapman, J. A. F. Hittinger, and S. Brunner, "Efficient simulation of 2+2-D multi-species plasmas waves using an Eulerian Vlasov code," Presented at APS Division of Plasma Physics Meeting (2013).

[29] S. Brunner, R. L. Berger, B. I. Cohen, L. Hausammann, and E. J. Valeo, Phys. Plasmas **21**, 102104 (2014).

[30] M. V. Goldman, Physics of Fluids **13**, 1281 (1970).

[31] R. L. Dewar, W. L. Kruer, and W. M. Manheimer, Phys. Rev. Lett. **28**, 215 (1972).

[32] R. L. Berger, S. Brunner, J. W. Banks, B. I. Cohen, and B. J. Winjum, Phys. Plasmas **22**, 055703 (2015), http://dx.doi.org/10.1063/1.4917482.

[33] W. L. Kruer, J. M. Dawson, and R. N. Sudan, Phys. Rev. Lett. **23**, 838 (1969).